

Transport Properties of Engineered Cementitious Composites under Chloride Exposure

by Mustafa Sahmaran, Mo Li, and Victor C. Li

This paper presents the results of an experimental investigation on the chloride transport properties of engineered cementitious composites (ECC) under combined mechanical and environmental loads. ECC is a newly developed, high-performance, fiber-reinforced cementitious composite with substantial benefit in both high ductility and improved durability due to tight crack width. By employing micromechanics-based material design, maximum ductility in excess of 3% under uniaxial tensile loading can be attained with only 2% fiber content by volume, and the typical single crack fracture behavior commonly observed in normal concrete or mortar is converted to multiple microcracking in ECC. In this study, immersion and salt ponding tests were conducted to determine chloride ion transport properties. Under high imposed bending deformation, the preloaded ECC beam specimens reveal microcracks less than 50 μm and an effective diffusion coefficient significantly lower than that of the similarly preloaded reinforced mortar beam because of the tight crack width control in ECC. In contrast, cracks larger than 150 μm are easily produced under the same imposed deformation and have significant effects on effective diffusion coefficient of reinforced mortar. Moreover, through the formation of microcracks, a significant amount of self-healing was observed within the ECC cracks subjected to NaCl solution exposure.

Keywords: chloride diffusivity; cracking; engineered cementitious composites.

INTRODUCTION

The corrosion of steel in concrete is one of the major problems with respect to the durability of reinforced concrete structures. The penetration of chloride ions into concrete is considered to be the major cause of corrosion. Generally, after casting concrete, a passivation film is formed surrounding the steel bars and protects them from corrosion initiation. Chloride ions, however, either from seawater or from deicing salt, will eventually penetrate the concrete cover and depassivate the protective film, and the embedded steel bars in concrete are no longer protected against corrosion in the presence of moisture and oxygen. When the steel bar starts to corrode, the volume of corrosion product exerts pressure on the concrete resulting in spalling of the concrete cover. Moreover, the cross section of reinforcing bar is diminished, thus reducing the load-carrying capacity of the concrete member.

The transport of chloride is a very complex phenomenon potentially involving different mechanisms, including permeation, diffusion, and absorption.¹ Depending on the conditions, transport of chloride may be driven by one or a combination of these three mechanisms. The main driving force behind permeation is the presence of a pressure gradient. Permeation is very important for concrete structures under water such as offshore structures. Absorption, driven by capillary pore suction, is the predominant transport process when the unsaturated concrete is exposed to chloride

solution. Diffusion is the most commonly studied transport process of chloride ions. When the saturated concrete is exposed to a chloride solution, a chloride concentration gradient is created between the concrete element surface and the pore solution. In this case, diffusion will be the predominant driving mechanism of chloride transport.

The development of reliable methods for predicting chloride transport into concrete is very important to determine the service life of a reinforced concrete structure. A number of studies have been carried out to understand the transport mechanism of chloride ions²⁻⁴ and numerous service-life prediction models have been introduced.⁴⁻⁷ In these studies, it is common to investigate the transport properties of uncracked concrete. Realistically, however, most reinforced concrete structures experience cracking in field conditions. Cracks in concrete structures may result from restrained shrinkage, thermal deformations, chemical reactions, poor construction practices, and mechanical loads.⁸

The formation of cracks increases the transport properties of concrete so that water, oxygen, and chloride ions easily penetrate and reach the reinforcing steel and accelerate the initiation of steel corrosion in concrete. Crack widths range from very small internal microcracks that occur on the application of a modest amount of stress, to quite large cracks caused by undesirable interactions with the environment.⁹ Wider crack widths have been found to induce corrosion much faster than relatively smaller ones. A comparison of diffusion coefficients for cracked and uncracked concrete shows an increase in the diffusion coefficient for cracked concrete by one or two orders of magnitude, with wider cracks resulting in higher values.¹⁰ Chloride diffusion in concrete precracked under three-point bending load was also studied by Gowripalan et al.¹¹ Prisms were preloaded up to a 0.3 mm (0.012 in.) crack width. The experiment showed that the apparent chloride diffusion coefficient is larger in the tensile than in the compression zone. Mangat and Gurusamy¹² studied the influence of cracks on chloride diffusion of steel fiber-reinforced concrete. Crack widths ranging between 70 to 1080 μm (0.003 to 0.043 in.) were produced on prism specimens and exposed to cycles of splash and tidal zone marine exposure. The authors concluded that crack widths larger than 500 μm (0.02 in.) have more pronounced influence on chloride intrusion whereas crack widths less than 200 μm (0.008 in.) appeared to have nearly no effect on chloride intrusion. The influence of crack width

ACI Materials Journal, V. 104, No. 6, November-December 2007.

MS No. M-2006-318 received August 2, 2006, and reviewed under Institute publication policies. Copyright © 2007, American Concrete Institute. All rights reserved, including the making of copies unless permission is obtained from the copyright proprietors. Pertinent discussion including authors' closure, if any, will be published in the September-October 2008 *ACI Materials Journal* if the discussion is received by June 1, 2008.

ACI member **Mustafa Sahmaran** is a Visiting Scholar in the Department of Civil and Environmental Engineering at the University of Michigan, Ann Arbor, MI, and a Research Assistant in the Department of Civil Engineering at the Middle East Technical University, Ankara, Turkey. He received his doctoral degree in civil engineering from the Middle East Technical University. His research interests include concrete technology, durability of concrete, and mineral and chemical admixtures.

Mo Li is a Doctoral Student Research Assistant in the Department of Civil and Environmental Engineering at the University of Michigan. She received her BS from Tongji University, Shanghai, China, and her MS from the University of Michigan. Her research interests include concrete repair durability, composite materials development for sustainable infrastructure, and using material methodology for improving durability of civil infrastructure.

ACI member **Victor C. Li** is a Professor in the Department of Civil and Environmental Engineering at the University of Michigan. He is a member of ACI Committee 544, Fiber Reinforced Concrete. His research interests include the design of ultra-ductile and green cementitious composites and their application to innovative infrastructure systems and integration of materials and structural design.

Table 1—Permissible crack widths for reinforced concrete under service loads

Exposure condition	Permissible crack width	
	in.	mm
Dry air or protective membrane	0.016	0.41
Humidity, moist air, soil	0.012	0.30
Deicing chemicals	0.007	0.18
Seawater and seawater spray, wetting and drying	0.006	0.15
Water-retaining structures	0.004	0.10

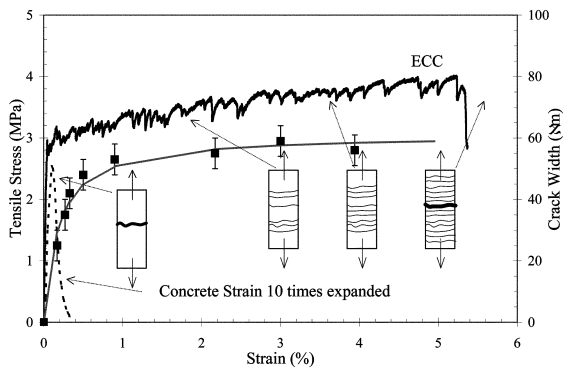


Fig. 1—Typical tensile stress-strain curve and crack width development of ECC.

up to 66 µm on chloride diffusivity was also studied by Tognazzi et al.¹³ The experimental results showed that the chloride diffusion coefficient through cracked concrete is proportional to the crack width. Aldea et al.¹⁴ performed rapid chloride permeability tests on normal- and high-strength concrete samples precracked under feedback-controlled splitting tensile tests, with crack widths up to 400 µm (0.016 in.). It was concluded that cracks less than 200 µm (0.008 in.) had no effect on chloride conductivity, whereas cracks between 200 and 400 µm (0.008 and 0.016 in.) resulted in higher chloride conductivity. According to ACI Committee 224, permissible crack widths at the tensile face of reinforced concrete structures for service loads under different environmental conditions are given in Table 1.⁸

ECC is a fiber-reinforced cement-based composite material micromechanically tailored to achieve high ductility and multiple cracking under tensile and shear loading.¹⁵⁻¹⁷ By employing micromechanics-based material design,^{15,18} maximum ductility in excess of 3% under uniaxial tensile

loading can be attained with only 2% by volume of short fibers. These properties, together with a relative ease of production including self-consolidation casting¹⁹ and shotcreting,²⁰ make them suitable for various civil engineering applications.

Figure 1 shows a typical uniaxial tensile stress-strain curve of an engineered cementitious composite (ECC) containing 2% polyvinyl alcohol (PVA) fiber. The characteristic strain-hardening after first cracking is accompanied by multiple microcracking. The crack width development during inelastic straining is also shown in Fig. 1. Even at ultimate load, the crack width remains on the order of 50 to 80 µm (0.002 to 0.003 in.). This tight crack width is self-controlled and, whether the composite is used in combination with conventional reinforcement or not, it is a material characteristic independent of reinforcing bar reinforcement ratio. In contrast, normal concrete and fiber-reinforced concrete rely on steel reinforcement for crack width control. The tight crack width of ECC is important to the durability of ECC structures as the tensile ductility is to the structural safety at ultimate limit state.

In actual field constructions, the high tensile strain capacity and multiple-cracking behaviors of ECC allow reduction of steel reinforcement ratio, but usually retain a limited amount for structural purposes. For this reason, it is important to test chloride transport properties of ECC. Little information exists on the transport of chloride ions in cracked and uncracked ECC. Miyazato and Hiraishi²¹ were probably the first to show that the penetration depth of chloride ions into ECC cover was substantially lower than that in concrete cover, for both beams preloaded to the same level of flexural deflection and subjected to accelerated chloride exposure. In the present research, experimental work was conducted on ECC beam specimens preloaded to different deformation levels. The microcracked specimens were then exposed to chloride ponding. In addition to ECC, the resistance to chloride ion penetration of cracked and uncracked reinforced (with steel wire mesh) mortar specimens were also measured in a control test series. The performance of cracked and uncracked ECC and mortar specimens, in terms of chloride penetration profile and depth, and effective diffusion coefficient as a function of beam deformation level, were compared. Immersion tests were also conducted on ECC and mortar cylinders to determine the chloride penetration depths as a function of immersion time.

RESEARCH SIGNIFICANCE

Concrete in real structures is often cracked. Durability is of increasing concern in the concrete industry, and it is significantly affected by the presence of cracks. The corrosion of reinforcing steel due to chloride ions in deicing salts or seawater is a major cause of premature deterioration of reinforced concrete structures. ECC is a newly-developed, high-performance, fiber-reinforced cementitious composite with substantial benefit in both high ductility and improved durability due to tight crack width. The main objective of this study was to quantify how cracking caused by mechanical loading influences the chloride transport properties of ECC, which may be used to predict changes in durability performance under service conditions. This kind of data can be used for service life prediction and life-cycle cost analysis of ECC structures, as well as providing a rational basis for the durable design of ECC infrastructure systems. The research is particularly relevant given the anticipation that this type of material may be used in the microcracked state during the service life of the structure.

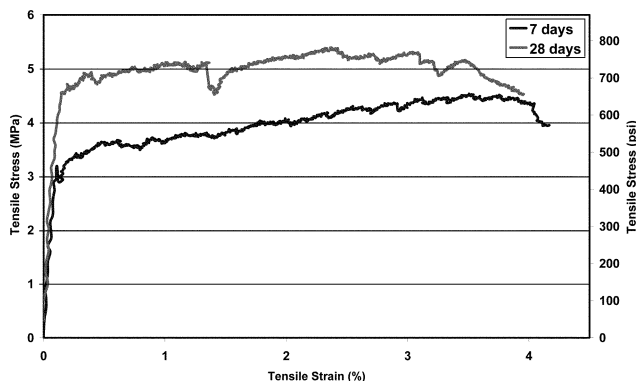


Fig. 2—Typical tensile stress-strain response of ECC mixture.

MATERIALS AND MIXTURE PROPORTIONS

The mixture proportions for ECC (M45) mixtures are summarized in Table 2. The components of ECC mixtures are similar to typical fiber-reinforced cement composites (FRCC), consisting of Type I portland cement, sand, Class F fly ash, water, fibers, and a high-range water-reducing admixture (HRWRA). Unlike typical FRCCs, however, the component characteristics and proportions within ECC are carefully determined through the use of micromechanical design tools¹⁷ to achieve the desired strain-hardening response. To minimize the mortar matrix fracture toughness, no large aggregates were used, and the silica sand had an average and maximum grain size of 110 μm (0.004 in.) and 200 μm (0.008 in.), respectively. The PVA fibers were purposely manufactured with a tensile strength, elastic modulus, and maximum elongation matching those needed for strain-hardening performance. Additionally, the surface of the PVA fibers was coated 1.2% by weight with a proprietary hydrophobic oiling agent to control the interfacial bonding properties between the fiber and matrix for strain-hardening performance.²² The mechanical and geometrical properties of the PVA fibers used in this study are shown in Table 3.

In addition to ECC, the resistance of cracked and uncracked reinforced (with steel wire mesh) mortar specimens to chloride ion penetration was also measured in a control test series. The mixture proportions of the mortar specimens are also shown in Table 2. The components of this material are Type I portland cement, water, and natural river sand. The ultimate tensile strain capacity of ECC and the compressive strength test results of ECC and mortar mixtures are also listed in Table 2. The compressive strength was computed as an average of three standard $\text{Ø}75 \times 150 \text{ mm}$ ($\text{Ø}3 \times 6 \text{ in.}$) cylinder specimens. To characterize the direct tensile behavior of the ECC mixtures, $152.4 \times 76.2 \times 12.7 \text{ mm}$ ($6.0 \times 3.0 \times 0.5 \text{ in.}$) coupon specimens were used. Direct tensile tests were conducted under displacement control at a loading rate of 0.005 mm/second (0.0002 in./second). The typical tensile stress-strain curves of the ECC mixtures are shown in Fig. 2.

TEST SPECIMEN PREPARATION AND TESTING

From each mixture $\text{Ø}75 \times 150 \text{ mm}$ ($\text{Ø}3 \times 6 \text{ in.}$) cylinders were prepared for the determination of chloride penetration depth (immersion test) and $355.6 \times 50.8 \times 76.2 \text{ mm}$ ($14 \times 2 \times 3 \text{ in.}$) prisms were prepared for the determination of chloride ion profiles and diffusion coefficient (salt ponding test). All specimens were demolded at the age of 24 hours and moisture cured in plastic bags at $95 \pm 5\%$ relative humidity (RH) at

Table 2—Mixture properties of ECC and mortar

	Mortar	ECC (M45)
<i>FA/C</i>	—	1.2
<i>w/cm*</i>	0.35	0.27
Water (W), kg/m^3 (lb/yd ³)	215 (362)	331 (558)
Cement (C), kg/m^3 (lb/yd ³)	614 (1035)	570 (961)
Fly ash (FA), kg/m^3 (lb/yd ³)	—	684 (1153)
Sand (S), kg/m^3 (lb/yd ³)	1535 (2585)	455 (767)
Fiber (PVA), kg/m^3 (lb/yd ³)	—	26 (44)
High-range water-reducing admixture (HRWRA), kg/m^3 (lb/yd ³)	—	5.1 (8.6)
7-day compressive strength, MPa (ksi)	36.6 (5.3)	37.8 (5.5)
28-day compressive strength, MPa (ksi)	42.9 (6.2)	53.3 (7.7)
7-day tensile strain capacity, %	—	3.90
28-day tensile strain capacity, %	—	3.10

**cm* = cementitious materials (cement + fly ash).

Table 3—Mechanical properties of PVA fiber

Nominal strength, MPa (ksi)	Apparent strength, MPa (ksi)	Diameter, μm (in.)	Length, mm (in.)	Young's modulus, GPa (ksi)	Elongation, %
1620 (235)	1092 (158)	39 (0.002)	8 (0.3)	42.8 (6200)	6.0

$23 \pm 2 \text{ }^\circ\text{C}$ for 7 days. The specimens were then air cured at $50 \pm 5\%$ RH at $23 \pm 2 \text{ }^\circ\text{C}$ until the age of 28 days for testing.

Immersion test

At the end of 28 days, all surfaces of the cylindrical specimens except their bottom sides were sealed by silicon coating so that chloride penetration could occur only in one direction. Afterwards, they were left in the laboratory for another day. At the age of 29 days, the cylinders were stored under continuous exposure to 3% NaCl solution at room temperature. The NaCl solution was replenished every month to maintain uniform concentration. After 30-, 60-, and 90-day immersion periods, one cylinder was taken out and split open before being sprayed with 0.1 N silver nitrate (AgNO_3) solution. Where chlorides have penetrated to at least approximately 0.15% by weight of cement,²³ silver chloride will precipitate and cause that portion of the sample to turn white, whereas the silver nitrate in the nonchloride penetrated zone turns brown.

Salt ponding test

The chloride ion profiles and diffusion coefficient of ECC were evaluated in accordance with AASHTO T259-80.²⁴ In addition to ECC, the same transport properties of mortar specimens were also determined in a control test series. Each mortar prism was reinforced with three levels of steel mesh to achieve cracks of varying controlled widths. At the age of 28 days, prism surfaces were abraded using a steel brush as required by AASHTO T259-80.²⁴ After abrasion application, the prisms were preloaded using a four-point bending test to obtain different crack widths. The ponding test was carried out with the preloaded specimens in the unloaded state. A small amount of crack closure occurred on unloading. To account for this, all crack width measurements are conducted in the unloaded stage. The widths of the crack were measured on the surface of the specimens by a portable microscope. The average width of the resulting crack was obtained through the measurement of the crack widths at five points.

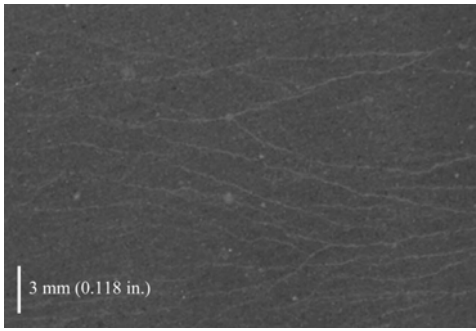


Fig. 3—Typical crack pattern on positive moment surface of ECC beams at 2 mm (0.079 in.) deformation.

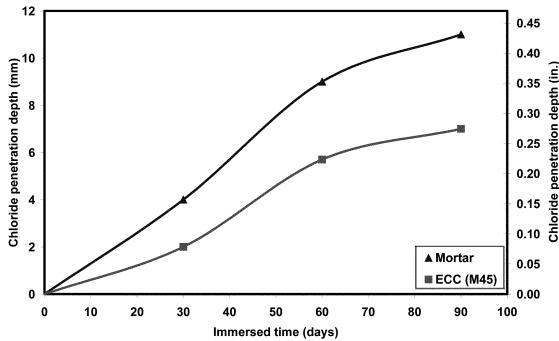


Fig. 4—Chloride penetration depth variation measured by immersion test.

Table 4 shows the preloaded beam deformation (BD) value, their corresponding average crack widths (CW), depths, and number of cracks for prism specimens. Two virgin prisms from each mixture were tested without preloading for control purposes. Note that preloading of the mortar beams were limited to 0.83 mm (0.033 in.) due to the large crack width (~400 μm [0.016 in.]) and crack depth of 70 mm (2.756 in.) generated in these specimens. In the ECC specimens, the crack width remains at approximately 50 μm even after beam deformation at 2 mm (0.079 in.). The crack length became impossible to measure accurately due to the tight crack width. Table 4 also shows the corresponding number of cracks for prism specimens at each beam deformation value. As seen from this table, when the deformation applied to the prism specimens is increased, the number of cracks on ECC is clearly increased but the crack width did not change for the different deformation values. Micromechanically designed ECC changes the cracking behavior from one crack with large width to multiple smaller cracks (Fig. 3).

After load application, plexiglass was used around the side surfaces of the prism to build an embankment for holding chloride solution on the exposed surface of prisms. At 29 days of age, a 3% NaCl solution was ponded on the cracked surface of the prisms. To retard the evaporation of the solution, aluminum plates were used to cover the top surface of the specimens. After 30 days of ponding, the salt solution was removed from the prism surface and samples were taken from each specimen for measuring chloride concentration with depth. In the case of virgin ECC and mortar specimens, a ponding test was also conducted after 90 days NaCl solution exposure in accordance with AASHTO T259-80.

Table 4—Crack widths, numbers, and depths of preloaded ECC and mortar prisms

Mixture ID	Beam deformation, mm (in.)	Average crack widths, μm (in.)	Crack depth, mm (in.)	Crack no.
Mortar	0.50 (0.020)	~50 (0.002)	20 (0.787)	1
	0.70 (0.028)	~150 (0.006)	36 (1.417)	1
	0.80 (0.031)	~300 (0.012)	55 (2.165)	1
	0.83 (0.033)	~400 (0.016)	70 (2.756)	1
ECC (M45)	0.5 (0.020)	~0	—	0
	1.0 (0.039)	~50 (0.002)	—	15
	1.5 (0.059)	~50 (0.002)	—	21
	2.0 (0.079)	~50 (0.002)	—	35

In the case of the mortar beams, it was found that chloride penetration concentrates where the precrack was located, and the penetration depth was deep, where approximately 40 to 70 mm (1.575 to 2.756 in.) depending on the crack width and crack depth of the specimen. Mortar powder samples were taken from the cracked zone for chloride analysis at various depths by using a 15 mm (0.591 in.) diameter rotary drill. In the case of the ECC beams, chloride penetration occurs at multiple locations corresponding to where the multiple cracks were formed during the preload. The penetration depth, however, was much shallower, between 0 and 40 mm (0 and 1.575 in.) depending on the level of imposed deformation. Powder samples for chloride analysis of cracked ECC specimens were taken where the multiple cracks were formed during the preload. Total chloride (acid-soluble) content by weight of material at each sampling point was examined according to AASHTO T 260-97.²⁵

The chloride profiles were then input into statistical and curve-fitting software. Equation (1), Crank's solution to Fick's second law, was fitted to the data.²⁶ The regression analysis yielded the values of the effective diffusion coefficient D_e and surface chloride concentration C_s for each specimen.

$$C_{(x,t)} = C_s \left[1 - \text{erf} \left(\frac{x}{2\sqrt{D_e t}} \right) \right] \quad (1)$$

where $C_{(x,t)}$ is the chloride concentration at time t at depth x ; C_s is the surface chloride concentration; D_e is the effective chloride diffusion coefficient; t is the exposure time; and $\text{erf}()$ is the error function.

This equation would perfectly describe the diffusion process of chlorides when no other transport mechanism of chloride ions (absorption and permeation) is present. This is not the case in real field conditions, however. In this experimental study, the coefficient of diffusion found by regression analysis of chloride profiles using Eq. (1) is referred to as effective diffusion coefficient D_e , which includes the combined transport mechanics. The value D_e forms a reasonable basis of comparing the diffusion properties of cracked and uncracked ECC and mortar specimens.

EXPERIMENTAL RESULTS AND DISCUSSION

The result of the immersion of the cylinders in the 3% NaCl solution up to 90 days is shown in Fig. 4. In this test, cylinder specimens were sealed by a silicon coating. Chloride ions were allowed to ingress only in one direction. The main transport mechanism in this test was absorption initially. After specimens become saturated, however, diffusion becomes the dominant transport mechanism at later ages.

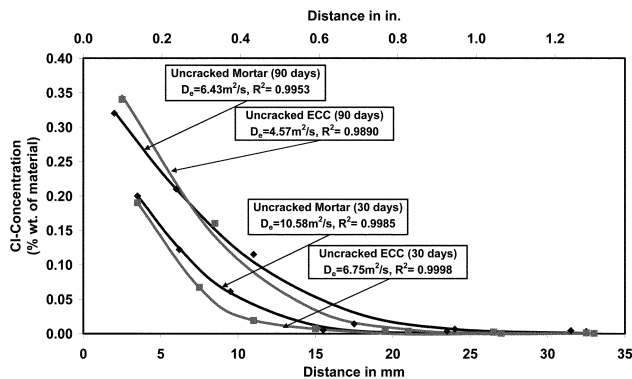


Fig. 5—Chloride profiles of uncracked mortar and uncracked ECC prisms after 30 and 90 days in 3% NaCl solution.

For ECC mixture containing a lower water-cementitious material ratio (w/cm) and high volume fly ash (FA), chloride ion penetration depths were always lower than that of the mortar mixture. The use of FA probably resulted in a denser matrix, by reducing the pore sizes and thickness of transition zone between fiber and surrounding cementitious matrix.

The chloride concentration profiles of uncracked mortar and uncracked ECC from the ponding test of prism specimens after 30 and 90 days of exposure, with the values of effective diffusion coefficients D_e and coefficient of determinations R^2 as determined by regression analysis, are shown in Fig. 5. The value of R^2 represents how well the estimated regression equation fits the data sample. A perfect fit of the equation and the data will have R^2 equal to one. The effective diffusion coefficients of the virgin mortar and ECC specimens calculated on the basis of 30 days of exposure are higher than that of 90 days of exposure likely due to the continuing hydration of cement and FA, which is beneficial in reducing pore sizes and densifying matrix.¹² In addition, the effective chloride diffusion coefficient of virgin ECC is lower than that of virgin mortar for 30 and 90 days, probably due to higher amounts of cementitious materials, lower w/cm , and high volume fly ash content. The use of fly ash reduces the coefficient of chloride diffusion due to the chloride binding effect of fly ash.²⁷ Intuitively, a lower effective chloride diffusion coefficient value is expected to increase the time to corrosion initiation, but service life prediction is beyond the scope of this paper.

The chloride concentration profiles of cracked mortar and cracked ECC, which were exposed to NaCl solution, are shown in Fig. 6. The chloride concentration profiles of virgin ($BD = 0$ mm) ECC and mortar specimens cured in the same environment and of same age are also included in this figure. The chloride contents at different depths from the exposed surface were determined after 30 days of exposure to the chloride environment. The chloride content in the cracked zone decreased with increasing depth. As seen from Fig. 6, the presence of cracks significantly modifies the chloride transport properties of reinforced mortar. In all cases, chloride concentrations increase with increasing crack widths, especially in deeper depths from the top of the reinforced mortar specimens. The increase is fairly high at crack widths larger than 150 μm (0.006 in.) for mortar specimens. These conclusions are consistent with previous research findings.¹² The multiple cracking in ECC due to preloading alters the transport properties measured as a function of beam

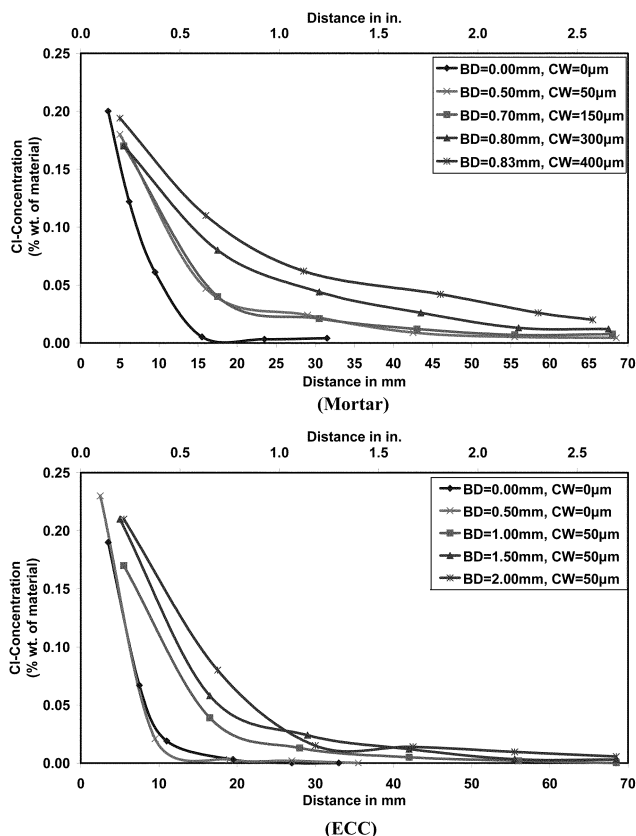


Fig. 6—Chloride profiles of mortar and ECC prisms in cracked zone at 30 days exposure.

Table 5—Chloride ponding test—effective diffusion coefficient

Mixture ID	Beam deformation, mm (in.)	Average crack widths, μm (in.)	Effective diffusion coefficient, $\text{m}^2/\text{second} \times 10^{-12}$ (in. ² /second $\times 10^{-8}$)
Mortar	0.00	—	10.58 (1.64)
	0.50 (0.020)	~50 (0.002)	33.28 (5.16)
	0.70 (0.028)	~150 (0.006)	35.54 (5.51)
	0.80 (0.031)	~300 (0.012)	126.53 (19.61)
	0.83 (0.033)	~400 (0.016)	205.76 (31.89)
ECC (M45)	0.00	—	6.75 (1.05)
	0.50 (0.002)	~0	8.10 (1.26)
	1.00 (0.039)	~50 (0.002)	27.99 (4.34)
	1.50 (0.059)	~50 (0.002)	37.50 (5.81)
	2.00 (0.079)	~50 (0.002)	54.22 (8.40)

deformation. It was found that chloride ingress increases as the number of cracks in ECC specimens increased. This increase, however, is relatively insignificant for ECC specimens when compared with mortar specimens at the same deformation levels. Thus, an ECC specimen with multiple microcracks exhibited a much increased chloride penetration resistance.

The effective chloride diffusion coefficients of prisms, calculated by using the chloride ion profiles mentioned previously, together with Fick's second law, are summarized in Table 5. As expected, this table clearly demonstrates the increase in effective diffusion coefficient with beam deformation and crack width increase in the mortar specimens. It was also found that the effective diffusion coefficient increased as the number of cracks in the ECC specimens

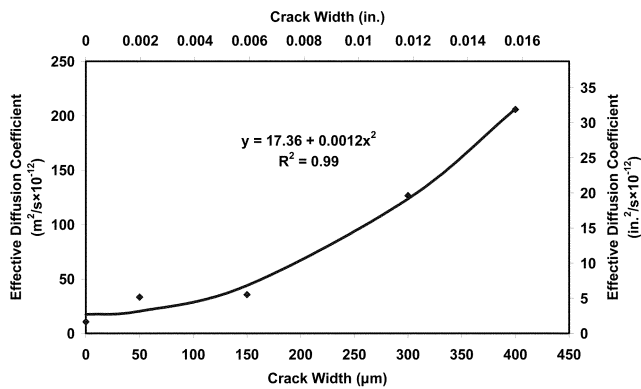


Fig. 7—Diffusion coefficient versus crack width for mortar deformed under bending load.

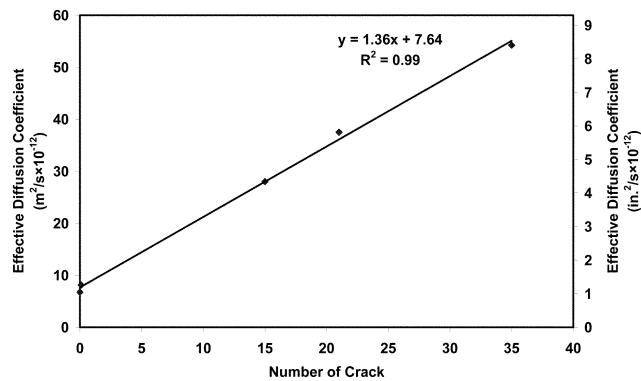


Fig. 8—Diffusion coefficient versus number of cracks for ECC.

increased. Cracks within the ECC specimens opened to a maximum width of approximately 50 µm (0.002 in.). As designed, the ECC specimens reveal a significantly smaller effective diffusion coefficient compared with the mortar specimens preloaded to the same deformation level, again reflecting the reduction in chloride ion transport rate as a result of tight crack width control in the ECC.

Figure 7 shows the relationship between the effective diffusion coefficient of chloride ions and crack widths in mortar specimens exposed to 30 days of NaCl solution. At the crack, salt solution may fill the crack and diffusion may also occur from the crack plane.¹¹ This is evident from the high chloride concentrations measured along the depth of the crack. The effective diffusion coefficient generally increased with increases in the crack width and became almost constant when the crack width fell below 150 µm (0.006 in.). It appears that the effective diffusion coefficient of mortar has the form of a power function of the crack width. The relationship between crack width and chloride diffusivity has also been examined by other researchers.^{12–14} Despite the numerous investigations, a consensus of the relationship between crack width and coefficient of diffusion has never been reached. The variety of experimental methods to create these cracks, the methods used to measure the chloride transport properties, the methods used to measure the chloride contents, and the reactivity of the chemical element within the solid body are the main reasons for the diversity of results obtained from these different studies.²⁸

In the case of mortar beams reinforced with three layers of steel mesh, pitting corrosion was also observed in the first

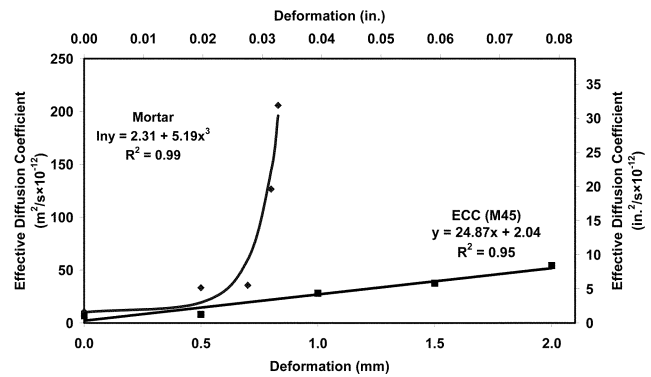


Fig. 9—Diffusion coefficient versus preloading deformation level for ECC and mortar.

layer of steel mesh of specimens having crack widths of 400 µm (0.016 in.) after 30 days of NaCl solution exposure. Therefore, cracks can reduce the service life of reinforced concrete structures by accelerating the initiation of corrosion especially when the crack width is larger than 150 µm (0.006 in.) when the diffusion coefficient picks up significantly.

For the ECC mixture, the crack width of all specimens for the different beam deformation level is the same. As seen from Fig. 1, even at large imposed deformation (2.0 mm [0.079 in.]), crack widths of ECC remain nearly constant after approximately 1% tensile straining, whereas the number of cracks on the tensile surface of the ECC specimens increased. For this reason, the effective diffusion coefficient of ECC specimens at different deflection levels, exposed to 30 days of NaCl solution, are plotted against the number of cracks in Fig. 8. Corresponding values for virgin ECC specimens cured in the same environment and of same age are also included in this plot. As the number of cracks along the specimen grows, the effective diffusion coefficient of ECC increased linearly with an increase in crack number, which is in agreement with research findings by Konin et al.²⁹

Figure 9 shows the relationship between the effective diffusion coefficient of chloride ions and the beam deformation level for mortar and ECC specimens. Despite the same or higher magnitude of imposed overall deformation and higher crack density, the ECC specimens reveal an effective diffusion coefficient considerably lower than that of the reinforced mortar because of the tight crack width control. Especially for the higher deformation level, the effective diffusion coefficient of mortar increased exponentially with beam deformation. The effective diffusion coefficient of ECC, however, increased linearly with the imposed deformation value because the number of microcracks on the tensile surface of ECC is proportional to the imposed beam deformation. The total chloride concentration profiles perpendicular to the crack path indicate no significant chloride penetration even at large imposed deformation (2 mm [0.079 in.]) for ECC specimens.

The reason for the relatively low diffusion coefficient of cracked ECC specimens is due to the tight crack width and the presence of self-healing of the microcracks. The self-healing of cracks becomes prominent when the crack width is small. Based on experimental results, Edvardsen³⁰ and Reinhardt and Jooss³¹ proposed that cracks with widths below 0.1 mm (0.004 in.) can be closed by a self-healing process. In the case of precracked ECC specimens exposed

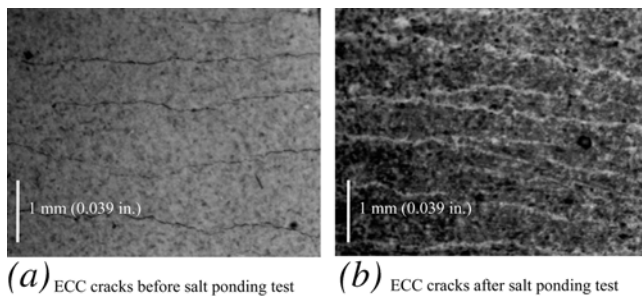


Fig. 10—Self healing products in ECC microcracks before and after salt ponding test at 30 days exposure.

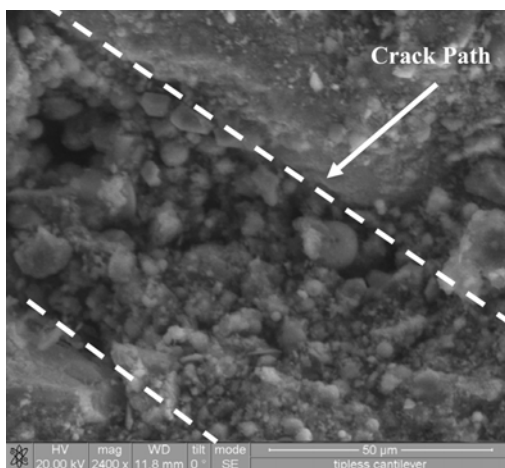


Fig. 11—ESEM micrograph of rehydration products in self-healed crack.

to salt solution, a distinct white deposit was visible over the crack surface at the end of a 1-month exposure period (Fig. 10). These deposits were most probably caused by efflorescence due to leaching of calcium hydroxide (CH) into cracks⁹ and due to the presence of NaCl ion in solution. This white deposit on the crack surface easily blocked the flow path due to the smaller crack width of ECC. An environmental scanning electron microscope (ESEM) observation of the fractured surface of ECC across a healed crack is shown in Fig. 11. The present ESEM observations show that most of the products seen in the cracks were newly formed C-S-H gels. CH and deposition of salts in the crack path were also observed. These results indicate that microcracks of ECC exposed to NaCl solution healed completely after exposure for 30 days to NaCl solution. This can be attributed primarily to the large fly ash content and relatively low water-binder ratio within the ECC mixture. The continued pozzolanic activity of fly ash is responsible for the self-healing of the crack, which reduces the ingress of the chloride ions.

CONCLUSION

The results obtained from the immersion test indicated that the performance of ECC in reducing chloride penetration depth was better than that of mortar after 30-, 60-, and 90-day immersion periods.

In the virgin beam specimens, the effective chloride diffusion coefficient of ECC was lower than that of mortar, probably due to higher amounts of cementitious materials, lower w/cm , and high volume FA content. When subjected to four-point bending loads, ECC and reinforced mortar beams exhibited

different cracking patterns and crack widths. Cracks with widths below 50 μm (0.002 in.) are distributed within the surface of the ECC specimens as a result of bending load. Even at large imposed deformation level, the crack width of ECC remains nearly constant, whereas the number of cracks increased. On the other hand, after bending load application, a single large crack is present on the mortar specimens. Especially at higher imposed deformation, ECC reveals an effective diffusion coefficient significantly lower than that of the reinforced mortar because of the tight crack width control. The effective diffusion coefficient of ECC was found to be linearly proportional to the number of cracks, whereas the effective diffusion coefficient of reinforced mortar is proportional to the square of the crack width. Therefore, the effect of the crack width on chloride transport was more pronounced when compared with that of the crack number. Additionally, through the formation of small microcracks, a significant amount of self-healing was observed within the ECC cracks subjected to NaCl solution, which aids in further reducing the effective diffusion coefficient of the microcracked ECC.

From the results of this study, it is concluded that ECC is effective in slowing the diffusion of chloride ion under combined mechanical and environmental (chloride exposure) loading, by virtue of its ability to achieve self-controlled tight crack width.

ACKNOWLEDGMENTS

The first author would like to acknowledge the financial support of TUBITAK (The Scientific and Technical Research Council of Turkey). This research was partially funded through an NSF MUSES Biocomplexity Program Grant (CMS-0223971 and CMS-0329416). MUSES (Materials Use: Science, Engineering, and Society) supports projects that study the reduction of adverse human impact on the total interactive system of resource use, the design and synthesis of new materials with environmentally benign impacts on biocomplex systems, as well as the maximization of efficient use of materials throughout their life cycles.

REFERENCES

1. Uji, K.; Matsuoka, Y.; and Maruya, T., "Formulation of an Equation for Surface Chloride Content of Concrete due to Permeation of Chloride," *Corrosion of Reinforcement in Concrete*, Society of Chemical Industry, London, UK, 1990, pp. 258-267.
2. Hong, K., and Hooton, R. D., "Effects of Cyclic Chloride Exposure on Penetration of Concrete Cover," *Journal of Cement and Concrete Research*, V. 29, No. 9, Sept. 1999, pp. 1379-1386.
3. Ababneh, A.; Benboudjema, F.; and Xi, Y., "Chloride Penetration in Nonsaturated Concrete," *Journal of Materials in Civil Engineering*, V. 15, No. 2, Mar.-Apr. 2003, pp. 183-191.
4. Hooton, R. D., and McGrath, P. F., "Issues Related to Recent Developments in Service Life Specifications for Concrete Structures," *Chloride Penetration into Concrete*, International RILEM Workshop, St. Remy-Les Chevreuse, 1995, 10 pp.
5. Clifton, J., "Predicting the Service Life of Concrete," *ACI Materials Journal*, V. 90, No. 6, Nov.-Dec. 1993, pp. 611-617.
6. Liang, M. T.; Wang, K. L.; and Liang, C. H., "Service Life Prediction of Reinforced Concrete Structures," *Journal of Cement and Concrete Research*, V. 29, No. 9, Sept. 1999, pp. 1411-1418.
7. ACI Committee 365, "Service-Life Prediction (ACI 365.1R-00)," American Concrete Institute, Farmington Hills, MI, 2000, 44 pp.
8. ACI Committee 224, "Control of Cracking in Concrete Structures (ACI 224R-01)," American Concrete Institute, Farmington Hills, MI, 2001, 46 pp.
9. Mindess, S.; Young, J. F.; and Darwin, D., *Concrete*, Prentice Hall Inc., Englewood Cliffs, NJ, 1981, 644 pp.
10. Raharinaivo, A.; Brevet, P.; Grimaldi, G.; and Pannier, G., "Relationship between Concrete Deterioration and Reinforcing-Steel Corrosion," *Durability of Building Materials*, V. 4, 1986, pp. 97-112.
11. Gowripalan, N.; Sirivivatnanon, V.; and Lim, C. C., "Chloride Diffusivity of Concrete Cracked in Flexure," *Journal of Cement and Concrete Research*, V. 30, No. 5, May 2000, pp. 725-730.

12. Mangat, P. S., and Gurusamy, K., "Chloride Diffusion in Steel Fibre Reinforced Marine Concrete," *Journal of Cement and Concrete Research*, V. 17, No. 3, May 1987, pp. 385-396.
13. Tognazzi, C.; Ollivier, J.-P.; Carcasses, M.; and Torrenti, J.-M., "Couplage Fissuration-Dégradation Chimique des Matériaux Cimentaires: Premiers Résultats sur les Propriétés de Transfert," *Ouvrages, géomatériaux et interactions*, C. Petit, G. Pijaudier-Cabot, and J. M. Reynouard, eds., Hermès, Paris, 1998, pp. 69-84.
14. Aldea, C. M.; Shah, S. P.; and Karr, A., "Effect of Cracking on Water and Chloride Permeability of Concrete," *Journal of Materials in Civil Engineering*, V. 11, No. 3, Aug. 1999, pp. 181-187.
15. Li, V. C., "ECC—Tailored Composites through Micromechanical Modeling," *Fiber Reinforced Concrete: Present and the Future*, Banthia et al., eds., CSCE, Montreal, QC, Canada, 1998, pp. 64-97.
16. Li, V. C., "On Engineered Cementitious Composites (ECC)—A Review of the Material and its Applications," *Journal of Advanced Concrete Technology*, V. 1, No. 3, 2003, pp. 215-230.
17. Li, V. C.; Wang, S.; and Wu, C., "Tensile Strain-Hardening Behavior of Polyvinyl Alcohol Engineered Cementitious Composite (PVA-ECC)," *ACI Materials Journal*, V. 98, No. 6, Nov.-Dec. 2001, pp. 483-492.
18. Lin, Z.; Kanda, T.; and Li, V. C., "On Interface Property Characterization and Performance of Fiber Reinforced Cementitious Composites," *Journal Concrete Science and Engineering*, RILEM, V. 1, No. 3, 1999, pp. 173-184.
19. Kong, H. J.; Bike, S.; and Li, V. C., "Development of a Self-Compacting ECC Employing Electrosteric Dispersion/Stabilization," *Journal of Cement and Concrete Composites*, V. 25, No. 3, Apr. 2003, pp. 301-309.
20. Kim, Y. Y.; Kong H. J.; and Li, V. C., "Design of Engineered Cementitious Composite Suitable for Wet-Mixture Shotcreting," *ACI Materials Journal*, V. 100, No. 6, Nov.-Dec. 2003, pp. 511-518.
21. Miyazato, S., and Hiraishi, Y., "Transport Properties and Steel Corrosion in Ductile Fiber Reinforced Cement Composites," *Proceedings of the Eleventh International Conference on Fracture*, Turin, Italy, Mar. 20-25, 2005.
22. Li, V. C.; Wu, C.; Wang, S.; Ogawa, A.; and Saito, T., "Interface Tailoring for Strain-Hardening Polyvinyl Alcohol-Engineered Cementitious Composite (PVA-ECC)," *ACI Materials Journal*, V. 99, No. 5, Sept.-Oct. 2002, pp. 463-472.
23. Otsuki, N.; Nagataki, S.; and Nakashita, K., "Evaluation of AgNO₃ Solution Spray Method for Measurement of Chloride Penetration into Hardened Cementitious Matrix Materials," *Construction and Building Materials*, V. 7, No. 4, 1993, pp. 195-201.
24. AASHTO, "Standard Method of Test for Resistance of Concrete to Chloride Ion Penetration," AASHTO T259-80, 2001.
25. AASHTO, "Standard Method of Test for Sampling and Testing for Chloride Ion in Concrete and Concrete Raw Materials," AASHTO T260-97, 2001.
26. Crank, J., *The Mathematics of Diffusion*, 2nd Edition, Oxford University Press, London, UK, 1975.
27. Wiens, U., and Schiessl, P., "Chloride Binding of Cement Paste Containing Fly Ash," *Proceedings of the 10th International Congress on the Chemistry of Cement*, V. 4, SINTEF, Trondheim, Norway, 1997.
28. Gerard, B.; Reinhardt, H. W.; and Breysse, D., "Measured Transport in Cracked Concrete," *Penetration and Permeability of Concrete*, H. W. Reinhardt, ed., RILEM Report 16, 1997, pp. 123-153.
29. Konin, A.; Francois, R.; and Arliguie, G., "Penetration of Chlorides in Relation to the Microcracking State into Reinforced Ordinary and High Strength Concrete," *Materials and Structures*, V. 31, No. 209, June 1998, pp. 310-316.
30. Edvardsen, C., "Water Permeability and Autogenous Healing of Cracks in Concrete," *ACI Materials Journal*, V. 96, No. 4, July-Aug. 1999, pp. 448-454.
31. Reinhardt, H. W., and Jooss, M., "Permeability and Self-Healing of Cracked Concrete as a Function of Temperature and Crack Width," *Journal of Cement and Concrete Research*, V. 33, No. 7, Mar. 2003, pp. 981-985.